Assessment of romosozumab efficacy in the treatment of postmenopausal osteoporosis: Results from a mechanistic PK-PD mechanostat model of bone remodeling

Madge Martin, Vittorio Sansalone, David M.L. Cooper, Mark Forwood, Peter Pivonka

Assessment of romosozumab efficacy in the treatment of postmenopausal osteoporosis: results from a mechanistic PK-PD mechanostat model of bone remodeling

Madge Martin[a,b], Vittorio Sansalone[b], David M. L. Cooper[c], Mark R. Forwood[d], Peter Pivonka[a]

[a] *School of Chemistry, Physics and Mechanical Engineering, Queensland University of Technology, 2 George St, Brisbane, QLD 4000, Australia*
[b] *Laboratoire Modélisation et Simulation Multi-Echelle (MSME), UMR CNRS 8208, Université Paris-Est Créteil, 61 avenue du Général de Gaulle, 94010 Créteil, France*
[c] *Department of Anatomy, Physiology and Pharmacology, University of Saskatchewan, 107 Wiggins Road, Saskatoon, SK, Canada*
[d] *School of Medical Science, Griffith University, Gold Goast, QLD 4222, Australia*

Keywords: romosozumab, bone remodeling, Frost's mechanostat, postmenopausal osteoporosis, pharmacokinetics, pharmacodynamics, patient-specific therapy

Declarations of Interest

The authors do not have anything to disclose.

Email address: madgeaudreymarie.martin@hdr.qut.edu.au (Madge Martin)

Assessment of romosozumab efficacy in the treatment of postmenopausal osteoporosis: results from a mechanistic PK-PD mechanostat model of bone remodeling

Abstract

This paper introduces a theoretical framework for the study of the efficacy of romosozumab, a humanized monoclonal antibody targeting sclerostin for the treatment of osteoporosis. We developed a comprehensive mechanistic pharmacokinetic-pharmacodynamic (PK-PD) model of the effect of drug treatment on bone remodeling in postmenopausal osteoporosis (PMO). We utilized a one-compartment PK model to represent subcutaneous injections of romosozumab and subsequent absorption into serum. The PD model is based on a recently-developed bone cell population model describing the bone remodeling process at the tissue scale. The latter accounts for mechanical feedback via incorporating nitric oxide (NO) and sclerostin (Scl) as biochemical feedback molecules. Utilizing a competitive binding model, where Wnt and Scl compete for binding to LRP5/6, allows to regulate anabolic bone remodeling responses. Here, we extended this model with respect to romosozumab binding to sclerostin. For the currently approved monthly injections of 210 mg, the model predicted a 6.59%, 10.38% and 15.25% increase in BMD at the lumbar spine after 6, 12 and 24 months, respectively. These results are in good agreement with the data reported in the literature. Our model is also able to distinguish the bone-site specific drug effects. For instance, at the femoral neck, our model predicts a BMD increase of 3.85% after 12 months of 210 mg injections, which is consistent with literature observations. Finally, our simulations indicate rapid bone loss after treatment discontinuation, indicating that some additional interventions

such as use of bisphosphonates are required to maintain bone.

Keywords: romosozumab, bone remodeling, Frost's mechanostat, postmenopausal osteoporosis, pharmacokinetics, pharmacodynamics, patient-specific therapy

1. Introduction

Bone remodeling is the concerted action of bone resorption and bone formation taking place throughout life. Cells involved in the bone remodeling process are osteoclast (bone resorbing cells), osteoblasts (bone forming cells) and osteocytes (cells embedded in the bone matrix) [1]. In particular, osteocytes have been identified as the conductors of bone remodeling. A key regulatory molecule in anabolic bone remodeling, sclerostin, is almost exclusively produced by osteocytes [2, 3]. Imbalanced bone remodeling is linked to bone pathologies, such as osteoporosis (OP). In OP, bone resorption outweighs bone formation which, consequently, induces a negative bone balance [4]. This leads to a gradual decline in bone mass and ultimately results in bone fractures. Clinical bone research is concerned with developing new drugs or combining different drugs able to halt or even reverse bone loss.

Sclerostin, encoded by the SOST gene, is an inhibitor of the canonical Wnt signaling pathway which has a pivotal role in skeletal development, adult skeletal homeostasis, and bone remodeling. Osteocytes produce sclerostin, and the latter binds to low-density lipoprotein receptor-related protein 5/6 (LRP5/6) expressed on osteoblasts and osteocytes. Receptor binding inhibits Wnt signaling and the anabolic β-catenin signaling pathway [5]. Sclerostin levels are directly linked to bone turnover and are negatively correlated to bone formation. Consequently, targeting sclerostin has great potential for controlling the anabolic axis of bone remodeling [6].

In the past decade, several studies assessed the therapeutic potential of sclerostin neutralizing antibodies on bone mass. A first study led by Warmington et al. in 2004 identified that treatment with a sclerostin monoclonal antibody

gave rise to significant BMD increases in adult mice and rats, including up to 64% in trabecular bone volume of the tibial metaphysis [7]. Since then, various studies investigated the administration of a sclerostin monoclonal antibody as a means to counter osteoporosis-induced bone loss [6, 8] or promote bone fracture healing [6, 9].

A humanized monoclonal antibody against sclerostin, called romosozumab is currently under phase 3 clinical trial. This drug has been developed by Amgen and UCB and is known under its commercial name EVENITY^{TM}. Romosozumab has a significantly positive impact on bone mass [10, 11], which led to approval of the drug in Japan, Canada, South Korea, US and the European Union. The approved adult dosage of romosozumab is 210 mg administered subcutaneously (SC) once a month for 12 months. Results of the effect of long-term romosozumab treatment on bone mass and turnover markers as well as its interaction with other signaling pathways are still lacking.

The efficacy of the anabolic treatment of PMO through the injection of romosozumab is not yet fully understood. Numerical modeling aims at filling this gap, as well as providing a long-term vision of the treatment. In particular, pharmacokinetics and pharmacodynamics (PK-PD) help understand how drugs are released into the system (pharmacokinetics) and interact with pharmacological target sites (here, the target is sclerostin) in order to exert an effect on biological systems (pharmacodynamics). PK-PD models have a great potential to better understand the effects of monoclonal antibodies on disease progression [12, 13]. Only a few studies have so-far developed PK-PD models for analyzing sclerostin antibody efficacy on disease progression in osteoporosis [14, 15]. While these two studies accurately reproduce the dynamics of bone turnover markers (BTMs) and bone mineral density (BMD), the scope of their models is limited. In particular they do not consider any mechanical aspects of bone, but treat bone tissue as a separate "compartment" to the BTMs. Different bone sites such as lumbar spine and femoral neck are modeled with different sets of parameters that are fitted to the experimental data. In contrast, work by Pivonka and co-workers have highlighted that it is relevant to link bone cellular

activities to respective BMD or bone volume fraction [16, 17, 18, 19]. Furthermore, we have recently shown that it is not necessary to treat different bone sites as different compartments in order to simulate differential drug effects [20] or hormonal changes [19]. One requires only a consistent mechanical formulation of bone tissue.

The present paper aims at development of a comprehensive mechanistic PK-PD model of the effects of romosozumab on bone remodeling in PMO. In particular, we are interested in drug efficacy. The model consists of a recently developed multiscale model of bone remodeling which quantitatively takes into account Frost's mechanostat theory [1]. The latter concept is translated into a biochemical feedback loop in which osteocytes respond to changes in mechanical environment by regulating production of sclerostin (Scl) and nitric oxide (NO). The sclerostin-driven anabolic feedback regulates osteoblast proliferation via Wnt signaling. On the other hand, NO catabolic feedback regulates RANKL expression on osteoblast precursor cells. A simplified competitive binding model including Wnt proteins, sclerostin and LRP5/6 receptors (Scl-Wnt-LRP5/6 pathway) was used in this analysis to drive osteoblast proliferation [19].

We further develop here a one compartment PK model of romosozumab. Utilizing binding affinities between Scl and romosozumab, we extended our Scl-Wnt-LRP5/6 competitive binding model towards another binding partner. The developed pharmacodynamic model is first calibrated on monthly injections of 210 mg as per the trial data for the lumbar spine from Langdahl et al. [21] to determine the elimination rate of the bound complex of sclerostin to its antibody. Model validation is then performed on a complementary set of data involving various bone sites and injection dosages [22, 11, 21] (see Section 3).

The paper is organized as follows. Firstly, Section 2 introduces the mechanistic PK-PD model of romosozumab effects on PMO. This section consists of a detailed description of a one-compartment model of subcutaneous injections of romosozumab (Subsection 2.1), a bone cell population model (BCPM) able to simulate PMO (Subsection 2.2), a competitive binding model of the Scl-Wnt-

LRP5/6 pathway and romosozumab (Subsection 2.3), and an overview of the numerical model implementation (Subsection 2.4). Numerical results are presented in Section 3 together with experimental data. The results are discussed and compared with findings in the literature in Section 4. A summary and conclusions are provided in Section 5.

2. Mechanistic PK-PD model of bone remodeling simulating the effect of romosozumab on PMO

2.1. PK-PD modelling of sclerostin antibody anabolic therapy

Pharmacokinetic-pharmacodynamic models are frameworks capturing the dynamics of the binding of a drug to its target in the body and the clearance of that drug. We define here a PK-PD model for romosozumab as a one-compartment PK model where the subcutaneous injection is accounted for by adding a depot (D), from which the drug is absorbed into the central compartment (i.e., serum). Fig. 1 describes the framework of our pharmocokinetic model. To our knowledge, there is currently no evidence that romosozumab binding to plasma proteins would prevent it from reaching bone tissue, which would motivate the need for an additional compartment.

The kinetics of the drug concentration in the depot $C^{\mathsf{D}}_{\mathsf{SclAb}}$ are described as follows:

$$\frac{dC^{\mathsf{D}}_{\mathsf{SclAb}}}{dt} = -k_a C^{\mathsf{D}}_{\mathsf{SclAb}}, \tag{1}$$

where k_a is the absorption coefficient of the monoclonal antibody into the serum. Our model is a quasi-equilibrium model derived from Michaelis-Menten kinetics. Hence, we assume that the formation of the complex of sclerostin with its specific antibody has a characteristic time that is negligible compared to absorption and elimination processes. This leads to the assumption that the antibody binding reaction is at equilibrium. Furthermore, the Michaelis-Menten model implies that the sclerostin concentration is small relative to that of the antibody [13]. The evolution of the sclerostin antibody concentrations in the depot ($C^{\mathsf{D}}_{\mathsf{SclAb}}$)

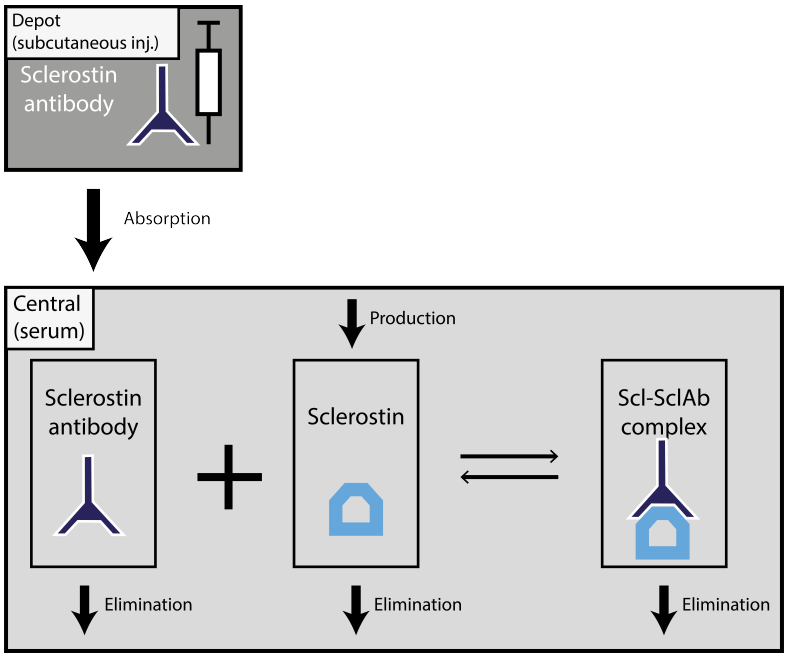

Figure 1: Schematic of the pharmacokinetic (PK) one-compartment model with depot for sclerostin antibody.

and in the central compartment ($C^{\mathsf{C}}_{\mathsf{SclAb}}$) are as follows:

$$\frac{dC^{\mathsf{C}}_{\mathsf{SclAb}}}{dt} = k_a C^{\mathsf{D}}_{\mathsf{SclAb}} - \left(\frac{V_{max}/(V_c/F)}{K_M + C^{\mathsf{C}}_{\mathsf{SclAb}}} + \tilde{D}_{\mathsf{SclAb}}\right) C^{\mathsf{C}}_{\mathsf{SclAb}}, \tag{2}$$

$$C^{\mathsf{C}}_{\mathsf{SclAb}}(t = t_0) = C^{\mathsf{C,res}}_{\mathsf{SclAb}}, \tag{3}$$

$$C^{\mathsf{D}}_{\mathsf{SclAb}}(t = t_0) = C^{\mathsf{D,res}}_{\mathsf{SclAb}} + \frac{\mathsf{Dose}}{V_c/F}, \ \mathsf{Dose} = \frac{\mathsf{Dose}^{\mathsf{mg}}}{M_{\mathsf{SclAb}}}, \tag{4}$$

where V_{max} is the maximum binding reaction velocity achieved by the system, K_M is the Michaelis constant, $\tilde{D}_{\mathsf{SclAb}}$ is the elimination rate of romosozumab (SclAb) and V_c/F is the volume of the central compartment adjusted for bioavailability. V_c is the central compartment volume and the factor F is the bioavailability approximated from literature [23, 24]. The latter is equal to 1 when the drug is administered intravenously. The administered dose is generally given in unit mass (we will use milligrams here), implemented here with the parameter $\mathsf{Dose}^{\mathsf{mg}}$. We note that all ligand receptor binding reactions and ligand levels pre-

sented in the following sections are evaluated with units pmol/L (pM). Hence, Eq. (4) classically uses the molar mass of romosozumab M_{SclAb} given in Evenity FDA Prescribing Information [25] (see Table 1) for the conversion of the dose $\mathsf{Dose}^{\mathsf{mg}}$. The initial concentration of drug in the central compartment and the depot are respectively accounted for via $C^{\mathsf{C,res}}_{\mathsf{SclAb}} \geq 0$ and $C^{\mathsf{D,res}}_{\mathsf{SclAb}} \geq 0$, indicating a potential remainder of drug resulting from previous injections.

Table 1: Typical parameter values for the one compartment PK model of romosozumab according to [25]. Values were either calculated from clinical data (C), obtained from an optimization based on clinical data (O) or retrieved from manufacturer data (M).

Symbol	Value	Unit	Definition	Source
k_a	0.450	day^{-1}	Absorption coefficient	O [23]
V_{max}	$1.50\,10^6$	ng.day^{-1}	Max. binding reaction velocity	O [23]
V_c	3.92	L	Central compartment volume	M [25]
F	0.692	-	Bioavailability	C [23]
K_M	$1.70\,10^3$	ng.mL^{-1}	Michaelis constant	O [23]
$\tilde{D}_{\mathsf{SclAb}}$	$6.00\,10^{-2}$	day^{-1}	Elimination rate	O [23]
M_{SclAb}	149	kDa	Molar mass	M [25]

The solution of Eq.(2) provides the romosozumab concentration in serum. The latter interacts with the osteocyte derived sclerostin concentration introduced in the next section (Equations (5)-(9)). Due to the fact that Eq.(2) is independent of the bone cell population model (BCPM), the equations governing drug kinetics (Equations (1)-(4)) can be solved independently. The concentration of drug in the depot at a given time point t is calculated by the algorithm explained in Appendix B.

The parameters defined in Table 1 are determined to reproduce the pharmocokinetic behavior of romosozumab, and therefore its effects on bone metabolism. While these parameters are specific to this drug, the model structure would allow to simulate the pharmacodynamics of any other anti-sclerostin monoclonal antibody, once PK parameters have been carefully adjusted against clinical data.

2.2. Bone cell population model (BCPM) of bone remodeling

The present work is based on the bone cell population model (BCPM) developed by Martin et al. [19]. The aim of the BCPM is to mechanistically describe the bone remodeling process at the tissue scale. Furthermore, the BCPM allows one to simulate the influence of biochemical and mechanical environments on bone remodeling together with imposing bone pathologies such as PMO onto the system. While previous attempts have been made to connect mechanical loading and biochemistry at the cellular scale [26, 27, 28, 29, 16, 18], our model is unique in the sense that it places the osteocytes as conductors of mechanical feedback which is biochemically actuated via nitric oxide (NO) and sclerostin (Scl). Furthermore, this model incorporates competitive binding reactions between Wnt, sclerostin and LRP5/6 which regulates proliferation of osteoblast precursor cells. This comprehensive model is schematically shown in Fig. 2.

Below, we briefly describe the main features of the model. A detailed description and mathematical formulation of all model features is presented in [19]. As seen in Fig. 2, four main signaling pathways are considered in order to describe the interactions between various bone cells and ligands involved in bone remodeling:

(a) RANK-RANKL-OPG catabolic pathway: regulates differentiation of osteoclasts;

(b) action of TGF-β implemented according to earlier studies [30, 16, 19]: upregulation of the differentiation of uncommitted osteoblasts (Ob_u), differentiation into osteoblast precursor cells (Ob_p), inhibition of differentiation of osteoblast precursor cells (Ob_p) and promotion of apoptosis of active osteoclasts (Oc_a);

(c) osteocyte mechanical feedback: described via nitric oxide (NO) catabolic regulation [31, 32, 33] and via sclerostin (Scl) anabolic regulation [6];

(d) Competitive binding of Wnt proteins and sclerostin (Scl) to LRP5/6 receptors on Ob_p: sclerostin is upregulated by osteocytes in response to

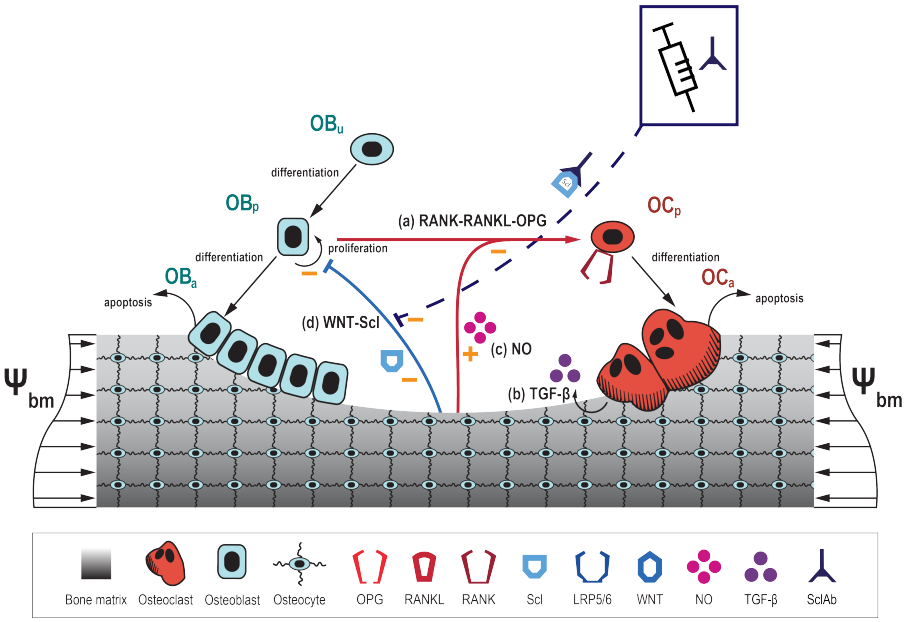

Figure 2: Overview of the bone cell population model (BCPM) containing both biochemical and mechanical feedback and their interaction with romosozumab (SclAb). Main regulating pathways of the model are: (a) Biochemical RANK – RANKL – OPG regulation (catabolic), (b) Biochemical TGF – β regulation (coupling). In this model Wnt and Scl compete for binding to LRP5/6 expressed on osteoblast precursor cells which regulates OB_p proliferation. Romosozumab interacts with the latter binding reactions to modify osteoblast precursor proliferation, (c) Mechanical NO regulation (catabolic), (d) Mechanical Scl-Wnt regulation (anabolic). Adapted from Martin et al. [19].

decreased mechanical loading [34, 35], and down-regulated by increased loads [36]. A comprehensive description of these binding reactions is given in Section 2.3.

As described in Martin et al. [19], macroscopic physiological loading of bone gives rise to stresses and strains in the bone matrix which are sensed by osteocytes. In our model, we use the strain energy density in the bone matrix (Ψ_{bm}) as a mechanical signal for osteocyte feedback (see Figs. 2,3). Osteocytes translate the mechanical loads into a biochemical feedback, i.e. catabolic feedback via nitric oxide (NO) and anabolic feedback via sclerostin (Scl). NO regulates

the RANKL expression on Ob_p and affects the RANKL/OPG ratio. Conversely, sclerostin interacts with Wnt-LRP5/6 to regulate Ob_p proliferation. For a detailed description of the micromechanical model for computing the strain energy density in the bone matrix (Ψ_{bm}), one can refer to [18]. Osteocyte production of NO and Scl relies on two sigmoidal regulatory functions defined in Appendix A, and the properties of the bone matrix and pores of the tissue (see Appendix C).

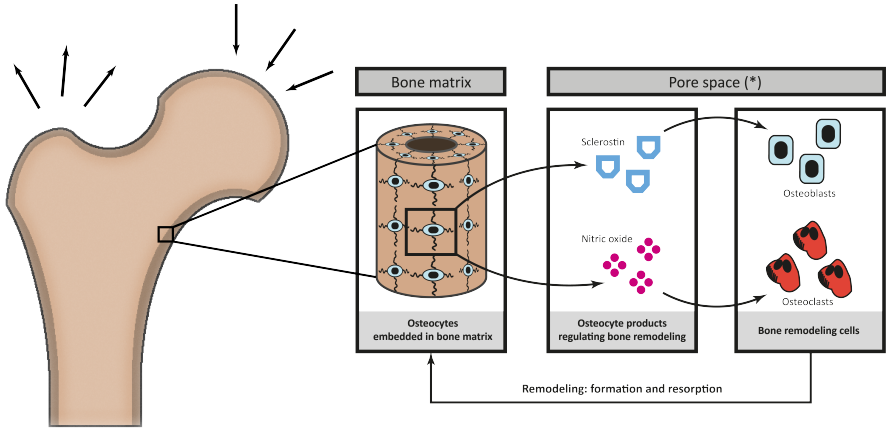

Figure 3: Overview of the regulation of the mechanobiological feedback by osteocytes through Scl and NO signaling. Scl regulates osteoblast precursors proliferation by inhibiting Wnt signaling (see Subsection 2.3). Romosozumab inhibits the anti-anabolic action of sclerostin by binding to sclerostin proteins. ($*$) Pore space refers here to cortical porosity and marrow spaces in trabecular bone.

The above described features of the BCPM can be presented by the following

evolution laws for bone cells [19]:

$$\frac{d\mathsf{Ob}_p}{dt} = D_{\mathsf{Ob}_u}\mathsf{Ob}_u\pi^{\mathsf{TGF}-\beta}_{\mathsf{act},\mathsf{Ob}_u} + P_{\mathsf{Ob}_p}\mathsf{Ob}_p\pi^{\mathsf{Wnt}}_{\mathsf{act},\mathsf{Ob}_p} - D_{\mathsf{Ob}_p}\mathsf{Ob}_p\pi^{\mathsf{TGF}-\beta}_{\mathsf{rep},\mathsf{Ob}_p} \quad (5)$$

$$\frac{d\mathsf{Ob}_a}{dt} = D_{\mathsf{Ob}_p}\mathsf{Ob}_p\pi^{\mathsf{TGF}-\beta}_{\mathsf{rep},\mathsf{Ob}_p} - \Delta_{\mathsf{Ob}_a}\mathsf{Ob}_a \quad (6)$$

$$\frac{d\mathsf{Oc}_a}{dt} = D_{\mathsf{Oc}_p}\mathsf{Oc}_p\pi^{\mathsf{RANK}}_{\mathsf{act},\mathsf{Oc}_p} - A_{\mathsf{Oc}_a}\mathsf{Oc}_a\pi^{\mathsf{TGF}-\beta}_{\mathsf{act},\mathsf{Oc}_a} \quad (7)$$

$$\frac{df_{\mathsf{bm}}}{dt} = k_{\mathsf{form}}\mathsf{Ob}_a - k_{\mathsf{res}}\mathsf{Oc}_a \quad (8)$$

$$\frac{d\mathsf{Ot}}{dt} = \eta\frac{df_{\mathsf{bm}}}{dt} \quad (9)$$

where D_{Ob_u}, D_{Ob_p} and D_{Oc_p} are differentiation rates of uncommitted osteoblast progenitor cells, osteoblast/osteoclast precursor cells, respectively. P_{Ob_p} denotes the proliferation rate of osteoblast precursor cells. Δ_{Ob_a} is the rate of clearance of active osteoblasts through apoptosis and differentiation. A_{Oc_a} is the apoptosis rate of active osteoclasts. Eq. (9) indicates that we assume that change in osteocyte population is proportional to the change in bone matrix volume fraction $\frac{df_{\mathsf{bm}}}{dt}$. The factor η indicates the average concentration of osteocytes embedded in the bone matrix. The aforementioned parameters are implemented as per Table 1 in the recent work of Martin et al. [19].

The various regulation mechanisms inherent to bone remodeling controlling the proliferation, differentiation or ligand production of cell populations are implemented classically via Hill functions: $\pi^{Y}_{\mathsf{act/rep},X}$. These functions are described in more detail in Appendix A.

2.3. Competitive binding Scl-Wnt-LRP5/6 interactions with romosozumab

In this section, we develop the implementation of the Scl-Wnt-LRP5/6 signalling pathway and its interactions with romosozumab. The competitive binding of Wnt and sclerostin proteins to the LRP5/6 receptor is complex. As depicted in Fig. 4(a), Wnt signaling is an anabolic pathway triggered by the binding of extracellular Wnt ligands to Frizzled and lipoprotein receptor-related proteins (LRP5/6) co-receptors on osteoblastic cell surfaces. This event triggers the intracellular activation of β-catenin, which promotes proliferation of

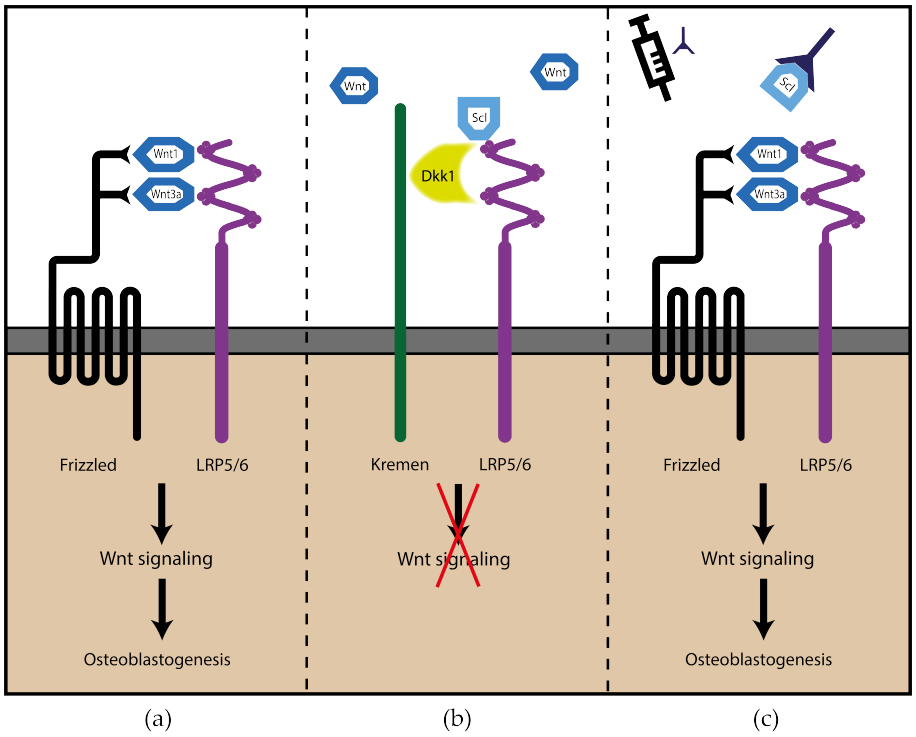

Figure 4: (a) Wnt ligands bind to Frizzled and LRP5/6 receptors, triggering Wnt signaling; (b) Dkk1 and Scl bind to LRP5/6 receptors, therefore inhibiting Wnt signaling; (c) The monoclonal antibody romosozumab (SclAb) binds to Scl, therefore preventing it from competitively binding to LRP5/6 receptors. Adapted from Martin et al. [19].

osteoblast precursor cells (among others). The formation of a Wnt-Frizzled-LRP5/6 complex is inhibited by the presence of sclerostin (Fig. 4(b)). Sclerostin (Scl) binds to LRP5/6 receptors, forming a complex with Kremen proteins and preventing Wnt signaling. Also note that literature suggests that sclerostin has a significantly higher affinity to LRP5/6 than Wnt [37, 38]. The latter fact was accounted for in our model via the values of the dissociation constants of the complexes Scl-LRP5/6 and Wnt-LRP5/6, as per Martin et al. [19]. This property highlights that, in presence of Scl, LRP5/6 receptors will be likely to bind faster to Scl than Wnt proteins. Note that, in the present study, the binding of Frizzled, Kremen and Dkk1, is not explicitly taken into account. We

only consider the dynamics of Scl binding as a first approximation, which has a similar affinity to the LRP5/6 receptors as Dkk1, according to experimental data [37]. We simplify the dynamics of the Wnt pathway: we do not account for the diversity of Wnt proteins and assume that Scl and Wnt bind directly to LRP5/6 as depicted in Fig. 2.

As explained earlier, the sclerostin antibody (SclAb) romosozumab has the potential to counteract bone loss by binding to sclerostin (see Fig. 4(c)). Based on the structure of our competitive binding model it is straightforward to include the action of romosozumab on Wnt-signaling. Romosozumab has a significantly higher affinity to sclerostin than sclerostin to LRP5/6 receptors [37, 38, 39], therefore promoting the Scl-SclAb binding over Scl-LRP5/6 binding.

In the present model, Wnt signaling affects osteoblast precursors proliferation via a multiplying factor $\pi^{\mathsf{Wnt}}_{\mathsf{act},\mathsf{Ob}_p}$ (Eq. (5)). This regulating function accounts for the LRP5/6 receptor occupancy, which translates the strength of Wnt/β-catenin signaling. Hence, one can calculate the ratio between $\mathsf{Wnt}-\mathsf{LRP5/6}$ complexes and the total concentration of LRP5/6 receptors $[\mathsf{LRP5/6}]_{\mathsf{tot}}$ – including the ones binding to sclerostin – as a function of the basal concentration of available Wnt proteins in the medium $[\mathsf{Wnt}]$, the total concentration $[\mathsf{LRP5/6}]_{\mathsf{tot}}$ of LRP5/6 receptors and the concentration of sclerostin $[\mathsf{Scl}]$:

$$\pi^{\mathsf{Wnt}}_{\mathsf{act},\mathsf{Ob}_p} = f^{\mathsf{Wnt}}([\mathsf{Wnt}], [\mathsf{Scl}], [\mathsf{LRP5/6}]_{\mathsf{tot}}), \tag{10}$$

where the concentrations of LRP5/6 ($[\mathsf{LRP5/6}]_{\mathsf{tot}} = N^{\mathsf{LRP5/6}}_{\mathsf{Ob}_p}\mathsf{Ob}_p$) and sclerostin ($[\mathsf{Scl}]$) are time-dependent and f^{Wnt} is implicitly defined by deriving the equation of the total concentration of LRP5/6 receptors, as per Martin et al. [19]. We assume here that the degradation of the complex Wnt-LRP5/6 is negligible and that bone marrow mesenchymal stem cells (uncommitted osteoblasts Ob_u, whose concentration is assumed to be constant in the model) are producing Wnt. Hence, we postulate here a basal concentration $[\mathsf{Wnt}]$ of available Wnt proteins in the medium. Model parameters are listed in Tables 2 and 3 in the recent work of Martin et al. [19].

Additionally, we work here under a steady-state assumption: the kinetics of the binding reactions are assumed to be fast compared to the processes they influence (namely, the cell population's evolution and ligand production). This assumption implies a balance between the production and degradation of sclerostin, leading to:

$$\begin{aligned} P_{\mathsf{Scl}} = &\quad \tilde{D}_{\mathsf{Scl}}[\mathsf{Scl}] + \tilde{D}_{\mathsf{Scl}\ \cdot\mathsf{LRP5/6}}[\mathsf{Scl}\cdot\mathsf{LRP5/6}] + \tilde{D}_{\mathsf{Scl}\ \cdot\mathsf{SclAb}}[\mathsf{Scl}\cdot\mathsf{SclAb}], \quad (11)\\ = &\quad \tilde{D}_{\mathsf{Scl}}[\mathsf{Scl}] + \tilde{D}_{\mathsf{Scl-LRP5/6}}\frac{[\mathsf{Scl}][\mathsf{LRP5/6}]}{K_D^{\mathsf{Scl-LRP5/6}}} + \tilde{D}_{\mathsf{Scl-SclAb}}\frac{[\mathsf{Scl}]C^{\mathsf{C}}_{\mathsf{SclAb}}}{K_D^{\mathsf{Scl-SclAb}}}, \quad (12)\end{aligned}$$

where the production of sclerostin P_{Scl} can be decomposed into a term accounting for body production $P_{\mathsf{Scl},b}$ and an additional term corresponding to the external dosage $P_{\mathsf{Scl},d}$. The external dosage term $P_{\mathsf{Scl},d}$ is set null in this paper as an injection of sclerostin is out of the scope of this paper. Therefore, the production of sclerostin reads as follows:

$$P_{\mathsf{Scl}} = P_{\mathsf{Scl},b} = \beta_{\mathsf{Scl,Ot}}\pi^{\Psi_{\mathsf{bm}}}_{\mathsf{rep,Scl}}[\mathsf{Ot}]\left(1-\frac{[\mathsf{Scl}]}{[\mathsf{Scl}]_{\mathsf{max}}}\right) \quad (13)$$

In the above equations, $\tilde{D}_X$ is the degradation rate of X, and $[\mathsf{Scl}]_{\mathsf{max}}$ is a saturation sclerostin concentration. Note that, in the expression of the body production of sclerostin (Eq. 13), the mechanical repressor function $\pi^{\Psi_{\mathsf{bm}}}_{\mathsf{rep,Scl}}$ regulates the local sclerostin production by osteocytes. As explained above, the concentration of unbound LRP5/6 receptors $[\mathsf{LRP5/6}]$ can be expressed as a function of the concentration of free sclerostin $[\mathsf{Scl}]$ (see Eq. (10)). As a result, the balance equation Eq. (11) can be written as a quadratic equation of unknown $[\mathsf{Scl}]$ as follows:

$$A[\mathsf{Scl}]^2 + B[\mathsf{Scl}] + C = 0, \quad (14)$$

where:

$$\begin{aligned} A &= \tilde{D}_{\mathsf{Scl}} + \tilde{D}_{\mathsf{Scl-SclAb}}\ \frac{C^{\mathsf{C}}_{\mathsf{SclAb}}}{K_D^{\mathsf{Scl-SclAb}}} + \frac{\beta_{\mathsf{Scl}}\ [\mathsf{Ot}]\ \pi^{\Psi_{\mathsf{bm}}}_{\mathsf{rep,Scl}}}{\mathsf{Scl}_{\mathsf{max}}} > 0, \quad (15)\\ B &= A\cdot K_D^{\mathsf{Scl-LRP5/6}}\ (1+\frac{[\mathsf{Wnt}]}{K_D^{\mathsf{Wnt-LRP5/6}}}) + \tilde{D}_{\mathsf{Scl-LRP5/65}}[\mathsf{LRP5/6}]_{\mathsf{tot}}\\ &\quad -(P_{\mathsf{Scl},d} + \beta_{\mathsf{Scl}}[\mathsf{Ot}]\pi^{\Psi_{\mathsf{bm}}}_{\mathsf{rep,Scl}}) \quad (16)\\ C &= -(P_{\mathsf{Scl},d} + \beta_{\mathsf{Scl}}[\mathsf{Ot}]\pi^{\Psi_{\mathsf{bm}}}_{\mathsf{rep,Scl}})\ (1+\frac{[\mathsf{Wnt}]}{K_D^{\mathsf{Wnt-LRP5/6}}}) < 0 \quad (17)\end{aligned}$$

We showed in a previous study that that Eq. (14) has one and only one physiologically sensible solution [19]. Therefore, the only admissible root to Eq. (14) allows to find the values of the concentration of free sclerostin, and consequently the LRP5/6 receptor occupancy.

Note that, in Equation (11), the complex degradation $\tilde{D}_{\mathsf{Scl-SclAb}}$ cannot be determined directly from a single injection PK study. A parametric study involving bone metabolism dynamics is therefore necessary (see Section 3).

2.4. Numerical implementation of the model of treatment of PMO with romosozumab

Numerical implementation. We used Matlab Stiff Differential Algebraic Equations solver to solve a system of differential equations consisting of the evolution laws of bone cells (Eqs. (5)-(9)) and that of the sclerostin antibody in the serum (Eq. (2)), as well as one algebraic equation governing the balance of RANKL (see [19, 40] for details).

Simulation of post-menopausal osteoporosis. We use a RANKL injection term of $P_{\mathsf{RANKL}} = 2\ \mathsf{pM}$ to simulate post-menopausal osteoporosis, and an exponential decay law for sclerostin degradation rate (see Appendix D) as implemented in our previous study [19]. This strategy is supported by experimental evidence of increased RANKL/OPG ratios in post-menopausal subjects [41, 42, 43]. Additionally, studies showed an increase of serum sclerostin in post-menopausal subjects [44, 45] while its expression (local mRNA levels) decreased in animal models [45]. The increase in RANKL ratio alone is not able to reproduce the biomarker profile of sclerostin, therefore justifying the assumption of a gradual modification of sclerostin degradation.

Bone density gain. Simulations give the evolution of the bone volume fraction f_{bm} as a consequence of the differential equations (2) and (5)-(9). We assume here the changes in bone matrix volume fraction f_{bm} from our model to be equal to the changes in the bone mineral density (BMD). Therefore, in order to

compare our model results with literature, we computed the bone density gain at an instant t using the following equation:

$$\mathsf{BDG}_{\%} = \frac{f_{\mathsf{bm}}(t) - f_{\mathsf{bm}}(\tau_{\mathsf{treat}})}{f_{\mathsf{bm}}(\tau_{\mathsf{treat}})}, \tag{18}$$

where τ_{treat} is defined as the instant when the simulated anabolic treatment with romosozumab starts.

Calibration of the PK-PD model. The pharmacokinetic (PK) model was calibrated against clinical data from Padhi et al. [23] for a subcutaneous injection dose of 3 mg/kg (see Figure 5). We assumed an average subject weight of 70 kg as per Evenity prescribing information [25]. The calibration of the PD model consisted in determining the complex elimination constant $\tilde{D}_{\mathsf{Scl{\cdot}SclAb}}$. To this end, we used one set of the lumbar spine trial data from Langdahl et al.[21], corresponding to 210 mg monthly injections for 12 months (Figure 7).

Validation of the model. We compare our numerical bone volume fraction (f_{bm}) results to experimental data from monthly romosozumab injections of 70 mg, 140 mg and 210 mg at the lumbar spine and the femoral neck [11, 22, 21]. As discussed in Martin et al., at homeostasis, each bone site is characterized by a different value of the bone matrix volume fraction and therefore a specific value of the habitual stress σ [19]. This relation between loading and the bone matrix volume fraction f_{bm} determines the bone turnover, i.e. the number of bone cells in the representative volume element (RVE). We assign different values for baseline bone volume fractions, i.e., $f^0_{\mathsf{bm}} = 12.5\%$ for lumbar spine (LS) and $f^0_{\mathsf{bm}} = 25\%$ for the femoral neck (FN), which are within ranges suggested in literature [46, 47] and compute the respective tissue-scale stress σ and associated cell numbers in steady state (see Table 2).

3. Simulation results

Validation of the PK model. We used the trial data from Padhi et al. [23] to calibrate and validate our PK model. Note that the model was calibrated for

Table 2: Steady state values of bone cell concentrations and tissue-scale stress σ for bone site-specific remodeling simulations. Baseline bone matrix volume fractions are $f^0_{\mathsf{bm}} = 12.5\%$ for lumbar spine (LS) and $f^0_{\mathsf{bm}} = 25\%$ for femoral neck (FN).

Symbol	Value	Unit
	Lumbar spine	
Ob^0_a	$9.382\,10^{-4}$	pM
Ob^0_p	$1.190\,10^{-3}$	pM
Ob^0_u	$1.000\,10^{-2}$	pM
Oc^0_a	$1.876\,10^{-5}$	pM
Oc^0_p	$5.592\,10^{-3}$	pM
σ_{LS}	-2.041	MPa
	Femoral neck	
Ob^0_a	$8.831\,10^{-4}$	pM
Ob^0_p	$1.114\,10^{-3}$	pM
Ob^0_u	$1.000\,10^{-2}$	pM
Oc^0_a	$1.766\,10^{-5}$	pM
Oc^0_p	$5.592\,10^{-3}$	pM
σ_{FN}	-4.405	MPa

a subcutaneous injection dose of 3 mg/kg (approved dose), while the 1, 5 and 10mg/kg injections doses served for validation. Note that the 3 mg/kg injection dose represented the approved recommended dosage for a 70 kg woman. In Fig. 5, we used the parameters listed in Table 1 to simulate the injections and observed the evolution of the serum sclerostin antibody concentration $C^{\mathsf{C}}_{\mathsf{SclAb}}$.

The sclerostin antibody concentration increases as the drug is absorbed from the depot, and is then degraded or bound to sclerostin, respectively via the elimination coefficient $\tilde{D}_{\mathsf{SclAb}}$ or via the Michaelis Menten kinetics with the constant K_M (see Figure 6).

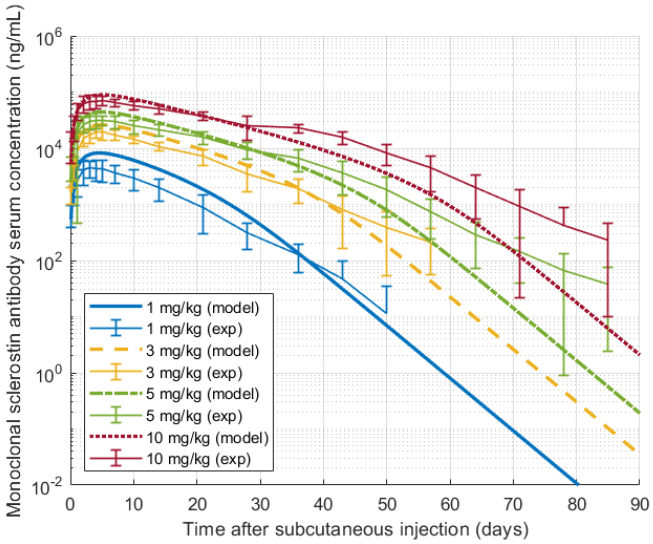

Figure 5: Evolution of sclerostin antibody levels in the central compartment (serum), for subcutaneous injections of 1, 3, 5 and 10 mg/kg: comparison of simulations (model) with experimental results (exp) from [23].

Subcutaneous romosozumab injection as a treatment for osteoporosis. In order to simulate the effects of a single sclerostin monoclonal antibody injection, we used our PK model to account for subcutaneous injections. In this study, we account for an advanced PMO state and the start of the treatment arbitrarily takes place 15 years after the start of PMO, corresponding approximately to the average age of the trial cohorts (around 70) [21, 22, 11].

In Figure 6, we start with an initial bone matrix fraction of 25% to simulate the drug dynamics in the femoral neck, and we model a single 210 mg injection. Figure 6 displays the evolution of sclerostin levels and bone volume fraction after the start of PMO (a), and sclerostin antibody levels in the depot and central compartments after injection (b). One can note that after one injection, the concentration of sclerostin antibody in serum is much higher than that of sclerostin (several orders of magnitudes higher (see Fig. 6 (a)).

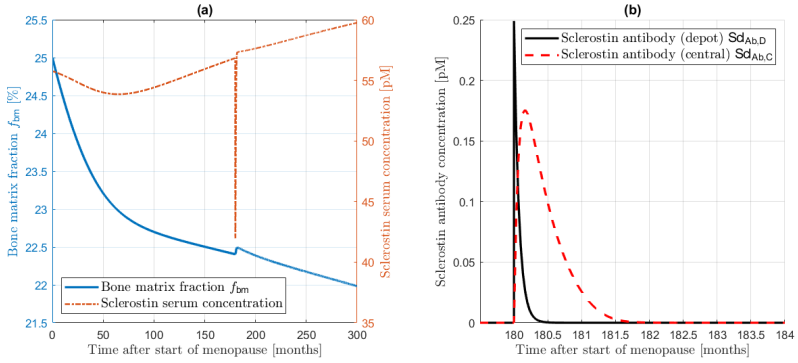

Figure 6: Simulation of PMO and a 210 mg single injection after 180 months (15 years) of PMO. Evolution of (a) sclerostin concentration and bone volume fraction (f_{bm}) (simulation, experimental data from Nordin et al. [48]) in the femoral neck ($f^0_{\mathsf{bm}} = 25\%$) and (b) sclerostin antibody levels in the depot and central compartments in the femoral neck as a function of the elapsed time since the start of PMO.

Calibration of the bound complex elimination constant. We performed the calibration of the bound complex elimination constant as displayed in Fig. 7. We simulated 12 monthly injections of 210 mg of sclerostin monoclonal antibody as per the trial data from Langdahl et al. [21]. We ran this simulation for various values of the complex elimination constant $\tilde{D}_{\mathsf{Scl{\cdot}SclAb}}$, observing the changes in bone volume fraction at the lumbar spine (LS).

In light of the results of the calibration study depicted in Fig. 7, we set the bound complex elimination constant to $\tilde{D}_{\mathsf{Scl{\cdot}SclAb}} = 3.2$ day^{-1}.

Monthly romosozumab injections: model validation. We confronted our model with other clinical trial data in the literature [22, 21, 11], as displayed in Fig. 8. We simulated the evolution of bone volume fraction in the femoral neck (FN) with monthly injections of 70 mg, 140 mg and 210 mg of romosozumab, and 210 mg for lumbar spine (LS).

We note that simulation results for the lumbar spine are in excellent agreement with the data of Langdahl et al. and McClung et al. [11, 21] (Fig. 8). Additionally, in both simulations ((a) and (b)), the BMD results for the Japanese

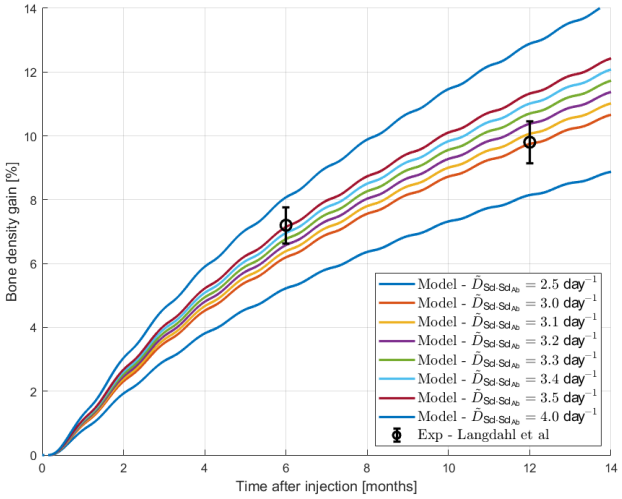

Figure 7: Evolution of bone volume fraction after the first injection in lumbar spine: simulation of monthly injections over a 14-month period, for different values of the bound complex elimination constant $\tilde{D}_{\mathsf{Scl\cdot SclAb}}$.

population lies somewhat higher [22], especially when considering lumbar spine. The model is also able to reproduce the bone loss after discontinuation of romosozumab treatment [11].

4. Discussion

Osteocytes mechanosensation. As mentioned previously, osteocytes, the most numerous cells in bone tissue (more than 90% of bone cells [49]), are thought to be responsible for the sensation of mechanical loads. They transduce the mechanical signals into biochemical signals orchestrating recruitment and activity of osteoblasts and osteoclasts. In the present study, we accounted for the influence of osteocyte mechanosensation by implementing their biochemical feedback, namely by modeling their expression of nitric oxide and sclerostin as a function of mechanical loading. In particular, we chose to follow the original idea of Scheiner et al. [18] who used the strain energy stored in the bone

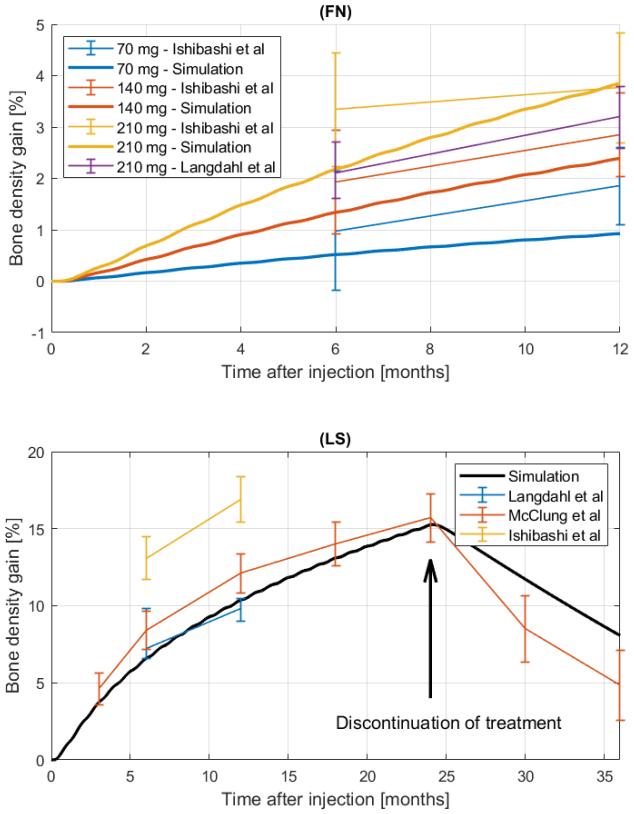

Figure 8: Simulations of PMO treatment with monthly injections of romosozumab: bone volume fraction f_{bm} (%) versus time (months): (top) femoral neck (FN) response (doses: 70 mg, 140 mg and 210 mg), and (bottom) lumbar spine (LS) response (dose: 24 monthly 210 mg injections, followed by placebo). Experimental data from Langdahl et al., McClung et al. and Ishibashi et al. [21, 11, 22].

matrix as a stimulus for osteocytes biochemical signalling. This assumption is an approximation to interpret the effects of mechanics on osteocytes. In fact, there exist several theories attempting to explain the mechanosensation of macroscopic loads by osteocytes, which rely on experiments and calculations involving physico-chemical mechanisms at the cellular scale. Main assumptions

emphasize the role of interstitial fluid flow, direct cell strain, streaming potentials or hydrostatic pressure as the most likely mechanisms for mechanosensation [50, 51, 52, 53, 54].

Description of the pharmacodynamics of romosozumab. The efficacy of romosozumab treatment is well represented by our model, as it can be observed in Fig. 8. One may notice that the results from Ishibashi et al. are different from the other studies we accounted for here. Ishibashi and coworkers focused their study on Japanese post-menopausal women, while Langdahl et al. and McClung et al. considered women from European and North American sites. [1]

Finkelstein et al. studied in 2002 the ethnic variation in bone mineral density in lumbar spine and femoral neck in premenopausal and early perimenopausal American women (mean age, 46.2 years) [55]. Their study demonstrated significant differences in bone mineral density and apparent density between ethnic groups. In particular, unadjusted lumbar spine BMD was 5% higher in the Caucasian than in the Japanese subjects, and when adjusting for covariates, the lumbar spine BMD was 3% lower in Caucasians than in Japanese. Unadjusted femoral neck BMD was 9% higher in Caucasians than in Japanese, and the adjusted values were very similar between those groups. These findings could explain the difference in evolution of BMD in the lumbar spine when comparing Ishibashi et al.'s data (Japanese population) with the results from McClung et al., Langdahl et al. as well as our model results.

Moreover, one may also note that the Japanese subjects may have a smaller volume of distribution, leading to different kinetics of the drug. Actually, in their FDA briefing document, the Bone, Reproductive and Urologic Drugs Advisory Committee states that "Romosozumab exposure is higher in subjects with lower body weight", which supports our hypothesis.

On romosozumab pharmacokinetics and pharmacodynamics. Our PK-PD model conforms to the dynamics of the drug absorption and elimination depicted in the

[1] McClung et al.'s study also comprised Latin American centres.

literature and predicts the expected impact on bone mass and sclerostin serum concentration (Fig. 5). On the other hand, our model uses Michaelis Menten kinetics which required the assumption that the concentration of sclerostin antibody is much higher than that of sclerostin at time of injection. Fig. 6 shows that this is indeed the case, as the concentration of sclerostin does not exceed about 10^2 pM, while the sclerostin antibody concentration does not get lower than about 10^4 pM during the treatment, which is two orders of magnitude higher.

On treatment planning. Our model allows us to simulate and therefore study the effects of romosozumab treatment on bone volume fraction. As an application, we investigated the changes in bone volume fraction after a certain time (6 months, 1 year, 2 years or 5 years), as a function of the monthly dose. This study is depicted in Figure 9.

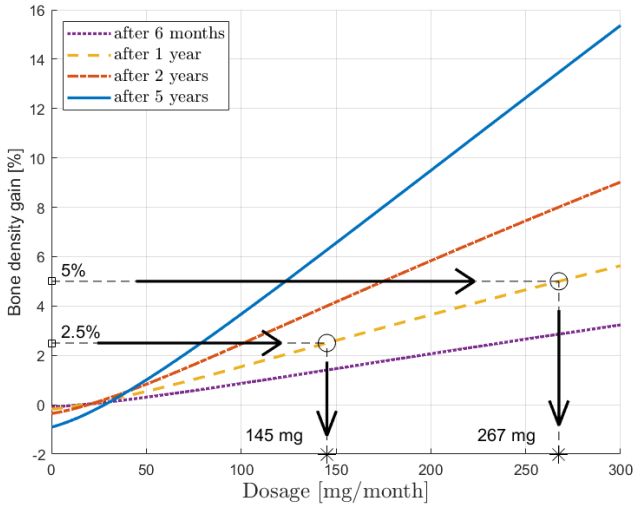

Figure 9: Influence of the dosage on the bone volume after 6 months, 1 year, 2 years and 5 years.

Firstly, one can observe that the bone gain at a given time point does not evolve linearly with the dosage. Hence, one interest of pharmacodynamics mod-

elling is to better predict the long-term effect of the treatment, and aim at a patient-specific therapy. In Figure 9, we take two examples. We assume a physician desires a 2.5% or a 5% bone density gain after 1 year of treatment. The values of the corresponding dosage of the treatment can be easily recovered graphically (145 mg and 267 mg, respectively). With our model, we can see that the dose necessary to achieve a 5% bone density gain is smaller than the double of the dose necessary to achieve a 2.5% bone density gain (267<145x2). This means that PK modelling allows minimization of doses and therefore minimization of side effects.

Note that the treatment does not seem to offset the bone loss due to postmenopausal osteoporosis when the dosage is not sufficiently high. This is highlighted in Figure 9. Under a 50 mg monthly dose, the bone gain after 5 years is below 1%. Additionally, one can see that for very small dosages (< 20 mg), the bone gain is negative, meaning that the treatment does not correct the negative bone balance.

Antibody injection and bone metabolism. One of the benefits of the present model is that it allows one to follow changes in cell numbers. Therefore, we are able to get a more comprehensive understanding of the remodeling process, in particular during the anabolic romosozumab treatment.

More specifically, Figure 10 depicts the changes subsequent to monthly romosozumab 210 mg injections in terms of (a) osteoclasts and osteoblasts cell numbers (directly linked to resorption and formation rates), (b) percentage of LRP5/6 receptor occupancy by Wnt proteins (evaluated through the Hill function $\pi^{\mathsf{Wnt}}_{\mathsf{act},\mathsf{Ob}_p}$), (c) sclerostin and nitric oxide expression and (d) serum levels.

As expected, osteoblast numbers increase following the first injection (a), as the receptor occupancy increases (b) while sclerostin serum levels decrease significantly (d). Bone gain arising from the treatment modifies the mechanical environment, resulting in an anti-anabolic osteocyte feedback reflected in an augmentation of sclerostin expression (c). Meanwhile, the variations in nitric oxide in terms of expression by osteocytes and serum levels stay small ($< 5\%$)

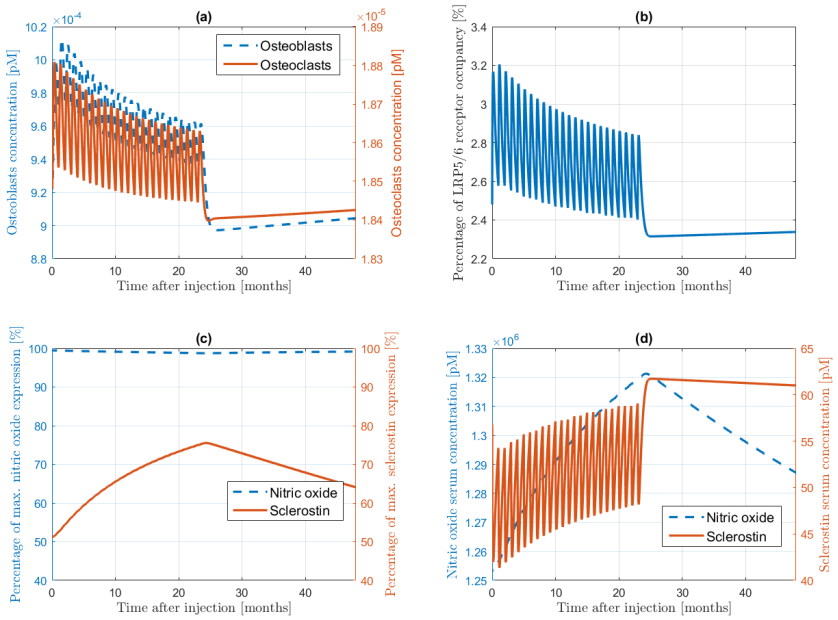

Figure 10: Evolution of osteoblasts and osteoclasts concentration (a), LRP5/6 occupancy by Wnt proteins $\pi^{\mathsf{Wnt}}_{\mathsf{act},\mathsf{Ob}_p}$ (b), percentage of maximum nitric oxide and sclerostin expression by osteocytes (c) and their serum levels (d), after the first injection of a 24 months treatment of 210 mg monthly subcutaneous injections (femoral neck).

in comparison to that of sclerostin (c,d).

Stolina et al. studied bone histomorphometry in ovariectomized rats receiving sclerostin antibody or vehicle [56]. They noticed a clear increase in bone formation markers and reduction of bone resorption parameters at 6 weeks. However, at 26 weeks, they noticed that, in comparison to controls, the increase of bone formation rate due to the antibody dropped (130% at 6 weeks, versus 74% at week 26), if adjusted with respect to bone surface (BFR/BS). This value corresponds to the actual bone forming activity of osteoblasts. In Figure 10(a), we also see clearly a diminished osteoblastic activity after a few months, in parallel with the decrease in LRP5/6 receptor occupancy.

We find here that the decrease in osteoblast numbers also coincides with

an increase in osteocytes expression of sclerostin as a result of the feedback regulation. This observation is consistent with Stolina et al.'s observations and hypotheses. Conversely, the changes in nitric oxide expression are very small (a few percents) compared to sclerostin expression by osteocytes, which increases significantly.

As highlighted in Subsection 2.1, our study reflects the pharmacodynamics of romosozumab based on its specific profile. However, the pharmacokinetics parameters listed in Table 1 could be modified in order to account for another sclerostin monoclonal antibody if necessary.

5. Conclusions

In the present paper, we introduced a target-mediated drug disposition model for sclerostin monoclonal antibody therapy and connected it to a bone remodeling model relying on osteocyte mechanosensation.

After calibration, the model was able to reproduce with good fidelity the bone gain induced by sclerostin antibody treatment reported in the literature.

Additionally, we observed that a main regulator of bone cell turnover during treatment was sclerostin expression by osteocytes. The increase in sclerostin expression during the treatment seems to be responsible for the decrease in bone formation markers after a few months of treatment. This mechanism is a result of the mechanostat, as the anabolic treatment shifts the mechanical stimulus (strain energy density in the bone matrix Ψ_{bm}, dependent on the tissue porosity) to a lower value, therefore increasing sclerostin production.

Our comprehensive mechanistic pharmacokinetic/pharmacodynamic modelling enabled the depiction of the relationship between bone gain and dosage. These results – and, more generally, our proposed framework – could help proposing more patient-specific treatment approaches.

This model offers the possibility to analyze different treatment options and how they could affect the efficacy of the treatment on bone gain. The present model is limited as it only focuses on bone tissue and bone cell pathways. In

this regard, potential side effects affecting other sites or pathways not taken into account in this model cannot be accounted for. Nonetheless, other limitations regarding the observation of mineralization or the combination with other drugs can definitely be adressed in the future.

6. Acknowledgements

Miss Madge Martin received a 12-month QUT School of Chemistry, Physics and Mechanical Engineering (CPME) Scholarship.

7. Declarations of Interest

The authors do not have anything to disclose.

Appendix A. Parameters and functions of the bone cell population model

In this section, we describe the parameters and functions used in the model to account for the effects of biochemistry on the remodeling process.

Cell differentiation, proliferation, apoptosis and ligand production are regulated by a number of binding reactions. These mechanisms are implemented with parameters displayed in Table 1 in the recent work of Martin et al. [19]. We account for main regulating pathways via the introduction of multiplicative regulatory Hill functions.

As described in earlier works [40], the up-regulation of X caused by the formation of the complex $L - R$ is defined by the ratio between the occupied receptors R by ligands L and the total number of receptors. Conversely, the repressor action of the receptor-ligand binding is the complementary of the promoting regulating function (see [40]). In the absence of competitive binding, under the previously-defined steady-state assumption, the up- and down- regu-

lating functions become the first-order Hill activator and repressor functions:

$$\pi^{L}_{\mathsf{act},X} = \frac{[L]}{K^{L-R}_{D,\mathsf{act}}+[L]} \tag{A.1}$$

$$\pi^{L}_{\mathsf{rep},X} = \frac{1}{1+\frac{[L]}{K^{L-R}_{D,\mathsf{rep}}}}, \tag{A.2}$$

where the coefficient $K^{L-R}_{D,\mathsf{act}}$ is the dissociation constant of the ligand-receptor binding reaction.

Additionally, we work here under a steady-state assumption: the kinetics of the binding reactions are assumed to be fast compared to the processes they influence (namely, the cell population's evolution and ligand production). Therefore, in line with Pivonka et al. [16], we find that the production rate P_L of a ligand L must be balanced with its degradation D_L, which itself can be assumed to be proportional to the concentration of L:

$$P_L + D_L = P_L - \sum_S \tilde{D}_{L-S}[L-S] = 0, \tag{A.3}$$

where $[L-S]$ represents the concentration of ligand L bound to S, a species in solution that can bind to L. The expressions of the production and degradation rates are detailed in an earlier work [19].

We also have the equilibrium of binding reactions:

$$[L][R] = K^{L-R}_{D,\mathsf{act}}[L-R], \tag{A.4}$$

where the coefficient $K^{L-R}_{D,\mathsf{act/rep}}$ is the dissociation constant of the ligand (L) - receptor (R) binding reaction.

The following binding reactions are considered, corresponding to the parameters listed in Tables 2 and 3 in the recent work of Martin et al. [19].

- Wnt and Scl binding competitively to LRP5/6 receptors, acting on pre-osteoblasts via $\pi^{\mathsf{Wnt}}_{\mathsf{act},\mathsf{Ob}_p}$;
- OPG binding to RANKL, as well as RANKL binding to RANK receptors, entering in RANKL balance to calculate the inhibiting influence through $\pi^{\mathsf{RANK}}_{\mathsf{act},\mathsf{Oc}_p}$;

- TGF-β binding to its receptors on osteoblasts and osteoclasts, whose concentration is proportional to the concentration of osteoclasts by a factor $\alpha_{\mathsf{TGF}-\beta} = 1.0\%$;

- NO and PTH acting on RANKL production by pre-osteoblasts via the function

$$\pi^{\mathsf{PTH,NO}}_{\mathsf{act/rep,RANKL}} = \lambda_s \left(\pi^{\mathsf{PTH}}_{\mathsf{act,RANKL}} + \pi^{\mathsf{NO}}_{\mathsf{rep,RANKL}}\right) + \lambda_c \; \pi^{\mathsf{PTH}}_{\mathsf{act,RANKL}} \pi^{\mathsf{NO}}_{\mathsf{rep,RANKL}},$$

  where NO is produced by osteocytes and PTH is assumed to be produced externally and has a constant concentration, and the respective contributions of the single and combined influence of the NO and PTH actions are $\lambda_s = 0.45$ and $\lambda_c = 0.90$;

- NO and Scl expression by osteocytes regulated by the mechanical stimulus Ψ_{bm} via functions $\pi^{\Psi_{\mathsf{bm}}}_{\mathsf{act,NO}}$ and $\pi^{\Psi_{\mathsf{bm}}}_{\mathsf{rep,Scl}}$ described below (Equations (A.5)-(A.6));

The mechanical feedback is driven by sigmoidal Hill functions as suggested by Peterson and Riggs [57]:

$$\pi^{\Psi_{\mathsf{bm}}}_{\mathsf{act,NO}} = \frac{{\Psi_{\mathsf{bm}}}^{\gamma_{\mathsf{act}}}}{\delta^{\gamma_{\mathsf{act}}}_{\mathsf{act}} + {\Psi_{\mathsf{bm}}}^{\gamma_{\mathsf{act}}}} \tag{A.5}$$

$$\pi^{\Psi_{\mathsf{bm}}}_{\mathsf{rep,Scl}} = \frac{{\Psi_{\mathsf{bm}}}^{\gamma_{\mathsf{rep}}}}{\delta^{\gamma_{\mathsf{rep}}}_{\mathsf{rep}} + {\Psi_{\mathsf{bm}}}^{\gamma_{\mathsf{rep}}}}, \tag{A.6}$$

where $\gamma_{\sim}$,$\delta_{\sim}$, are respectively the sigmoidicity term influencing the steepness of response and the value of the stimulus that produces the half-maximal response [57]. These parameters are listed in Table 4 in the recent work of Martin et al. [19]. In this previous work, the role of multiple model parameters was investigated, in particular with respect to anabolic and catabolic mechanical regulations of bone remodeling. The anabolic response was assessed with the simulation of post-menopausal osteoporosis, while the catabolic response was assessed with the simulation of space flight.

Appendix B. Modeling of multiple romosozumab injections

To calculate the amount of romosozumab in the depot (i.e. subcutaneous tissue) and the serum at any given time t, we use the algorithm schematically described in Figure B.11. Before the first injection we set $C^{\mathsf{D}}_{\mathsf{SclAb}}$ to zero. At the time of the first injection, the concentration of drug in the depot is $C^{\mathsf{D}}_{\mathsf{SclAb}} = C^{\mathsf{D,res}}_{\mathsf{SclAb}}$, as defined in Eq. (4). This value is $C^{\mathsf{D,res}}_{\mathsf{SclAb}} = 0$ at the start of the simulation. For each subsequent injection, that value is updated taking into account the remaining amount of drug from the previous injections after its absorption into the central compartment (coefficient k_a). After the last injection, the concentration of drug is calculated accounting for the absorption of the amount of drug present at the time of the last injection.

Hence, at each time point, we are able calculate the time derivative of $C^{\mathsf{C}}_{\mathsf{SclAb}}$ using Equation (2), where we insert the calculated value of $C^{\mathsf{D}}_{\mathsf{SclAb}}$.

Appendix C. Properties of matrix and fluid in the micro-mechanical model

The stiffness tensor of the extravascular bone matrix reads as follows (Kelvin notation):

$$\mathbb{c}_{\mathsf{bm}} = \begin{pmatrix} 18.5 & 10.3 & 10.4 & 0 & 0 & 0 \\ 10.3 & 20.8 & 11.0 & 0 & 0 & 0 \\ 10.4 & 11.0 & 28.4 & 0 & 0 & 0 \\ 0 & 0 & 0 & 12.9 & 0 & 0 \\ 0 & 0 & 0 & 0 & 11.5 & 0 \\ 0 & 0 & 0 & 0 & 0 & 9.3 \end{pmatrix} \text{GPa} \tag{C.1}$$

The stiffness tensor of the saturating fluid is:

$$\mathbb{c}_{\mathsf{vas}} = k_{\mathsf{H_2O}}\mathbb{J} + \mu_{\mathsf{H_2O}}\mathbb{K}, \tag{C.2}$$

where the bulk modulus and the shear modulus are respectively $k_{\mathsf{H_2O}} = 2.3$ GPa and $\mu_{\mathsf{H_2O}} = 0$ GPa, and $\mathbb{J}$ is the volumetric part of the fourth-order unit tensor $\mathbb{I}$, and $\mathbb{K}$ is its deviatoric part, $\mathbb{K} = \mathbb{I} - \mathbb{J}$.

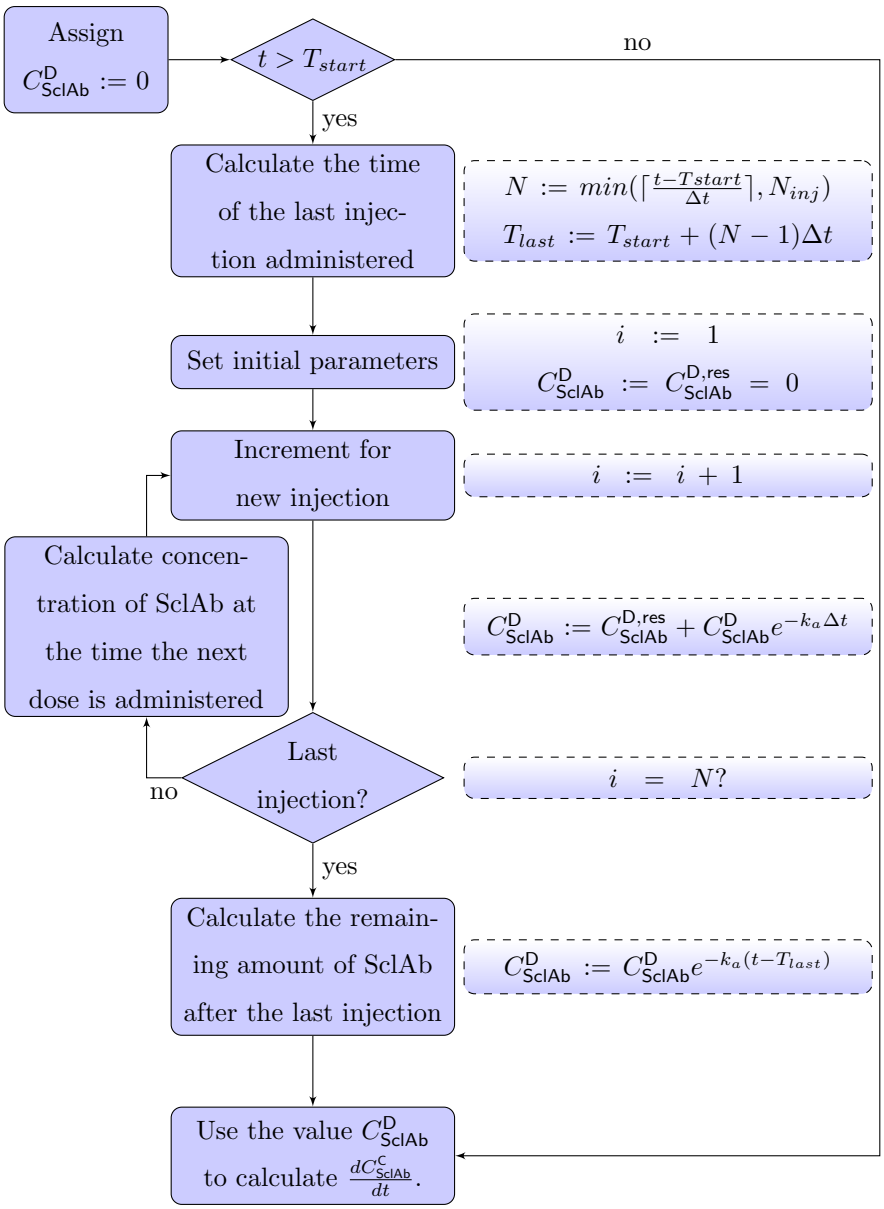

Figure B.11: Flow chart of the calculation of the amount of monoclonal antibody in the depot at the current time t. In the diagram, N is the number of the last injection that has been administered (as opposed to N_{inj}, the total number of injections of the simulated treatment), occurring at T_{last}, $C^{\mathsf{D}}_{\mathsf{SclAb}}$ is the concentration of antibody in the depot, i is the injection number, k_a is the absorption coefficient of the drug, and Δt is the time between two injections.

Appendix D. Modelling the degradation rate of sclerostin in PMO

Following a previous work, we assumed an exponential decay of the degradation rate of sclerostin: $\tilde{D}_{\mathsf{Scl}}(t = t_{menop} + \tau) = \tilde{D}_{\mathsf{Scl,PMO}}(\tau)$, where $\tilde{D}_{\mathsf{Scl,PMO}}$ is the function defined in Equation (D.1):

$$\tilde{D}_{\mathsf{Scl,PMO}}(\tau) = \tilde{D}^0_{\mathsf{Scl}}\,\mathsf{exp}(-\frac{\tau}{\tau_{PMO}}), \tag{D.1}$$

where $\tau_{PMO} = 20\mathsf{yr}$.

With this model of PMO, Martin et al. [19] showed that one can retrieve the increase of serum sclerostin reported in post-menopausal subjects [44, 45] and the decrease in sclerostin expression (local mRNA levels) found in animal models of menopause [45].

Appendix E. Nomenclature

The abbreviations used in the present paper are summarized in Table E.3.

References

[1] H. M. Frost, Bone "mass" and the "mechanostat": A proposal, The Anatomical Record 219 (1) (1987) 1–9. doi:10.1002/ar.1092190104.

[2] R. L. van Bezooijen, B. A. Roelen, A. Visser, L. van der Wee-Pals, E. de Wilt, M. Karperien, H. Hamersma, S. E. Papapoulos, P. ten Dijke, C. W. Löwik, Sclerostin Is an Osteocyte-expressed Negative Regulator of Bone Formation, But Not a Classical BMP Antagonist, The Journal of Experimental Medicine 199 (6) (2004) 805–814. doi:10.1084/jem.20031454.

[3] D. G. Winkler, M. K. Sutherland, J. C. Geoghegan, C. Yu, T. Hayes, J. E. Skonier, D. Shpektor, M. Jonas, B. R. Kovacevich, K. Staehling-Hampton, M. Appleby, M. E. Brunkow, J. A. Latham, Osteocyte control of bone formation via sclerostin, a novel BMP antagonist., The EMBO journal 22 (23) (2003) 6267–76. doi:10.1093/emboj/cdg599.

[4] B. Langdahl, S. Ferrari, D. W. Dempster, Bone modeling and remodeling: potential as therapeutic targets for the treatment of osteoporosis, Therapeutic Advances in Musculoskeletal Disease 8 (6) (2016) 225–235. doi:10.1177/1759720X16670154.

[5] L. F. Bonewald, M. L. Johnson, Osteocytes, mechanosensing and Wnt signaling, Bone 42 (4) (2008) 606–615. doi:10.1016/j.bone.2007.12.224.

[6] D. Ke, D. Padhi, C. Paszty, Sclerostin is an Important Target for Stimulating Bone Formation, Restoring Bone Mass and Enhancing Fracture Healing, Bone 46 (2010) S15. doi:10.1016/j.bone.2010.01.022.

[7] K. Warmington, S. Morony, I. Sarosi, J. Gong, P. Stephens, D. G. Winkler, M. K. Sutherland, J. A. Latham, H. Kirby, A. Moore, M. Robinson, P. J. Kostenuik, W. S. Simonet, D. L. Lacey, C. Paszty, Sclerostin Antagonism in Adult Rodents, via Monoclonal Antibody Mediated Blockade, Increases Bone Mineral Density and Implicates Sclerostin as a Key Regulator of Bone Mass During Adulthood, Journal of Bone and Mineral Research 19 (2004) S56–57.

[8] D. Padhi, B. Stouch, G. Jang, L. Fang, M. Darling, H. Glise, M. K. Robinson, S. S. Harris, E. Posvar, Anti-Sclerostin Antibody Increases Markers of Bone Formation in Healthy Postmenopausal Women, Journal of Bone and Mineral Research 22 (1) (2007) S37–S37.

[9] B. Kruck, E. A. Zimmermann, S. Damerow, C. Figge, C. Julien, D. Wulsten, T. Thiele, M. Martin, R. Hamdy, M. K. Reumann, G. N. Duda, S. Checa, B. M. Willie, Sclerostin neutralizing antibody treatment enhances bone formation but does not rescue mechanically induced delayed healing, Journal of Bone and Mineral Research 33 (9) (2018) 1686–1697.

[10] A. Markham, Romosozumab: First Global Approval, Drugs 79 (4) (2019) 471–476. doi:10.1007/s40265-019-01072-6.

[11] M. R. McClung, J. P. Brown, A. Diez-Perez, H. Resch, J. Caminis, P. Meisner, M. A. Bolognese, S. Goemaere, H. G. Bone, J. R. Zanchetta, J. Maddox, S. Bray, A. Grauer, Effects of 24 Months of Treatment With Romosozumab Followed by 12 Months of Denosumab or Placebo in Postmenopausal Women With Low Bone Mineral Density: A Randomized, Double-Blind, Phase 2, Parallel Group Study, Journal of Bone and Mineral Research 33 (8) (2018) 1397–1406. doi:10.1002/jbmr.3452.

[12] Y. Cao, W. J. Jusko, Incorporating target-mediated drug disposition in a minimal physiologically-based pharmacokinetic model for monoclonal antibodies, Journal of pharmacokinetics and pharmacodynamics 41 (4) (2014) 375–387. doi:10.1007/s10928-014-9372-2.

[13] P. Dua, E. Hawkins, P. H. van der Graaf, A Tutorial on Target-Mediated Drug Disposition (TMDD) Models, CPT: Pharmacometrics & Systems Pharmacology 4 (6) (2015) 324–337. doi:10.1002/psp4.41.

[14] R. Eudy, M. Gastonguay, K. Baron, M. Riggs, Connecting the dots: Linking osteocyte activity and therapeutic modulation of sclerostin by extending a multiscale systems model, CPT: Pharmacometrics & Systems Pharmacology 4 (9) (2015) 527–536. doi:10.1002/psp4.12013.

[15] C. C. Tang, C. Benson, J. McColm, A. Sipos, B. Mitlak, L. J. Hu, Population Pharmacokinetics and Pharmacodynamics of Blosozumab, in: American Conference on Pharmacokinetics, Arlington, Virginia, USA, 2015, pp. W–15.

[16] P. Pivonka, J. Zimak, D. W. Smith, B. S. Gardiner, C. R. Dunstan, N. A. Sims, T. John Martin, G. R. Mundy, Model structure and control of bone remodeling: A theoretical study, Bone 43 (2) (2008) 249–263. doi:10.1016/j.bone.2008.03.025.

[17] P. Pivonka, J. Zimak, D. W. Smith, B. S. Gardiner, C. R. Dunstan, N. A. Sims, T. John Martin, G. R. Mundy, Theoretical investigation of the role of

the RANK–RANKL–OPG system in bone remodeling, Journal of Theoretical Biology 262 (2) (2010) 306–316. doi:10.1016/j.jtbi.2009.09.021.

[18] S. Scheiner, P. Pivonka, C. Hellmich, Coupling systems biology with multiscale mechanics, for computer simulations of bone remodeling, Computer Methods in Applied Mechanics and Engineering 254 (2013) 181–196. doi:10.1016/j.cma.2012.10.015.

[19] M. Martin, V. Sansalone, D. M. L. Cooper, M. R. Forwood, P. Pivonka, Mechanobiological osteocyte feedback drives mechanostat regulation of bone in a multiscale computational model, Biomechanics and Modeling in Mechanobiology 18 (2019) 1475–1496. doi:10.1007/s10237-019-01158-w.

[20] J. Martínez-Reina, P. Pivonka, Effects of long-term treatment of denosumab on bone mineral density: insights from an in-silico model of bone mineralization, Bone 125 (2019) 87–95. doi:10.1016/j.bone.2019.04.022.

[21] B. L. Langdahl, C. Libanati, D. B. Crittenden, M. A. Bolognese, J. P. Brown, N. S. Daizadeh, E. Dokoupilova, K. Engelke, J. S. Finkelstein, H. K. Genant, S. Goemaere, L. Hyldstrup, E. Jodar-Gimeno, T. M. Keaveny, D. Kendler, P. Lakatos, J. Maddox, J. Malouf, F. E. Massari, J. F. Molina, M. R. Ulla, A. Grauer, Romosozumab (sclerostin monoclonal antibody) versus teriparatide in postmenopausal women with osteoporosis transitioning from oral bisphosphonate therapy: a randomised, open-label, phase 3 trial, The Lancet 390 (10102) (2017) 1585–1594. doi:10.1016/S0140-6736(17)31613-6.

[22] H. Ishibashi, D. B. Crittenden, A. Miyauchi, C. Libanati, J. Maddox, M. Fan, L. Chen, A. Grauer, Romosozumab increases bone mineral density in postmenopausal Japanese women with osteoporosis: A phase 2 study, Bone 103 (2017) 209–215. doi:10.1016/j.bone.2017.07.005.

[23] D. Padhi, G. Jang, B. Stouch, L. Fang, E. Posvar, Single-dose, placebo-controlled, randomized study of AMG 785, a sclerostin monoclonal antibody, Journal of Bone and Mineral Research 26 (1) (2011) 19–26. doi:10.1002/jbmr.173.

[24] D. M. Paton, MONOGRAPH, Drugs of the Future 39 (8) (2014) 553–556. doi:10.1358/dof.2014.39.8.2164452.

[25] Evenity [Prescribing Information], Thousand Oaks, California (2019). URL https://www.pi.amgen.com/{~}/media/amgen/repositorysites/pi-amgen-com/evenity/evenity{_}pi{_}hcp{_}english.ashx

[26] V. Klika, F. Marsík, A thermodynamic model of bone remodelling: The influence of dynamic loading together with biochemical control, Journal of musculoskeletal and neuronal interactions 10 (2010) 220–30.

[27] S. V. Komarova, R. J. Smith, S. J. Dixon, S. M. Sims, L. M. Wahl, Mathematical model predicts a critical role for osteoclast autocrine regulation in the control of bone remodeling, Bone 33 (2) (2003) 206–215. doi:10.1016/S8756-3282(03)00157-1.

[28] S. Maldonado, S. Borchers, R. Findeisen, F. Allgöwer, Mathematical modeling and analysis of force induced bone growth, Conference proceedings: ... Annual International Conference of the IEEE Engineering in Medicine and Biology Society. IEEE Engineering in Medicine and Biology Society. Annual Conference 1 (2006) 3154–3157. doi:10.1109/IEMBS.2006.260532.

[29] M.-I. Pastrama, S. Scheiner, P. Pivonka, C. Hellmich, A mathematical multiscale model of bone remodeling, accounting for pore space-specific mechanosensation, Bone 107 (2018) 208–221. doi:10.1016/j.bone.2017.11.009.

[30] V. Lemaire, F. L. Tobin, L. D. Greller, C. R. Cho, L. J. Suva, Modeling the interactions between osteoblast and osteoclast activities in bone

remodeling, Journal of Theoretical Biology 229 (3) (2004) 293–309. doi:10.1016/j.jtbi.2004.03.023.

[31] X. Fan, E. Roy, L. Zhu, T. C. Murphy, C. Ackert-Bicknell, C. M. Hart, C. Rosen, M. S. Nanes, J. Rubin, Nitric Oxide Regulates Receptor Activator of Nuclear Factor-κB Ligand and Osteoprotegerin Expression in Bone Marrow Stromal Cells, Endocrinology 145 (2) (2004) 751–759. doi:10.1210/en.2003-0726.

[32] J. W. M. Chow, S. W. Fox, J. M. Lean, T. J. Chambers, Role of Nitric Oxide and Prostaglandins in Mechanically Induced Bone Formation, J Bone Miner Res 13 (6) (1998) 1039–1044. doi:10.1359/jbmr.1998.13.6.1039.

[33] G. Zaman, a. a. Pitsillides, S. C. F. Rawlinson, R. F. L. Suswillo, J. R. Mosley, M. Z. Cheng, L. a. M. Platts, M. Hukkanen, J. M. Polak, L. E. Lanyon, Mechanical Strain Stimulates Nitric Oxide Production by Rapid Activation of Endothelial Nitric Oxide Synthase in Osteocytes, J Bone Miner Res 14 (7) (1999) 1123–1131. doi:10.1359/jbmr.1999.14.7.1123.

[34] A. Gaudio, P. Pennisi, C. Bratengeier, V. Torrisi, B. Lindner, R. A. Mangiafico, I. Pulvirenti, G. Hawa, G. Tringali, C. E. Fiore, Increased sclerostin serum levels associated with bone formation and resorption markers in patients with immobilization-induced bone loss, J Clin Endocrinol Metab 95 (5) (2010) 2248–2253. doi:10.1210/jc.2010-0067.

[35] J. M. Spatz, M. N. Wein, J. H. Gooi, Y. Qu, J. L. Garr, S. Liu, K. J. Barry, Y. Uda, F. Lai, C. Dedic, M. Balcells-Camps, H. M. Kronenberg, P. Babij, P. D. Pajevic, The Wnt inhibitor sclerostin is up-regulated by mechanical unloading in osteocytes in vitro, J Biol Chem 290 (27) (2015) 16744–16758. doi:10.1074/jbc.M114.628313.

[36] A. G. Robling, P. J. Niziolek, L. A. Baldridge, K. W. Condon, M. R. Allen, I. Alam, S. M. Mantila, J. Gluhak-Heinrich, T. M. Bellido, S. E. Harris, C. H. Turner, Mechanical stimulation of bone in vivo reduces osteocyte

expression of Sost/sclerostin., The Journal of biological chemistry 283 (9) (2008) 5866–75. doi:10.1074/jbc.M705092200.

[37] X. Li, Y. Zhang, H. Kang, W. Liu, P. Liu, J. Zhang, S. E. Harris, D. Wu, Sclerostin binds to LRP5/6 and antagonizes canonical Wnt signaling, J Biol Chem 280 (20) (2005) 19883–19887. doi:10.1074/jbc.M413274200.

[38] E. Bourhis, C. Tam, Y. Franke, J. F. Bazan, J. Ernst, J. Hwang, M. Costa, A. G. Cochran, R. N. Hannoush, Reconstitution of a Frizzled8-Wnt3a-LRP6 signaling complex reveals multiple Wnt and Dkk1 binding sites on LRP6, J Biol Chem 285 (12) (2010) 9172–9179. doi:10.1074/jbc.M109.092130.

[39] IUPHAR BPS Guide to Pharmacology, Romosozumab.
URL http://www.guidetopharmacology.org/GRAC/LigandDisplayForward?tab=biology{&}ligandId=8092

[40] P. Pivonka, P. Buenzli, C. Dunstan, A systems approach to understanding bone cell interactions in health and disease, in: S. Gowder (Ed.), Cell Interaction, IntechOpen, Rijeka, 2012, Ch. 7, pp. 169–204. doi:10.5772/51149.

[41] S. Jabbar, J. Drury, J. N. Fordham, H. K. Datta, R. M. Francis, S. P. Tuck, Osteoprotegerin, RANKL and bone turnover in postmenopausal osteoporosis, J Clin Pathol 64 (4) (2011) 354–357. doi:10.1136/jcp.2010.086595.

[42] U. Lerner, Bone Remodeling in Post-menopausal Osteoporosis, J Dent Res 85 (7) (2006) 584–595. doi:10.1177/154405910608500703.

[43] M. McClung, Role of RANKL inhibition in osteoporosis, Arthritis Res Ther 9 (SUPPL.1) (2007) 1–6. doi:10.1186/ar2167.

[44] M. S. M. Ardawi, H. A. Al-Kadi, A. A. Rouzi, M. H. Qari, Determinants of serum sclerostin in healthy pre- and postmenopausal women, Journal of Bone and Mineral Research 26 (12) (2011) 2812–2822. doi:10.1002/jbmr.479.

[45] S. Jastrzebski, J. Kalinowski, M. Stolina, F. Mirza, E. Torreggiani, I. Kalajzic, H. Y. Won, S.-K. Lee, J. Lorenzo, Changes in bone sclerostin levels in mice after ovariectomy vary independently of changes in serum sclerostin levels, Journal of Bone and Mineral Research 28 (3) (2013) 618–626. doi:10.1002/jbmr.1773.

[46] E. Legrand, D. Chappard, C. Pascaretti, M. Duquenne, S. Krebs, V. Rohmer, M.-F. Basle, M. Audran, Trabecular bone microarchitecture, bone mineral density, and vertebral fractures in male osteoporosis, Journal of Bone and Mineral Research 15 (1) (2000) 13–19. doi:10.1359/jbmr.2000.15.1.13.

[47] A. Nazarian, J. Muller, D. Zurakowski, R. Müller, B. D. Snyder, Densitometric, morphometric and mechanical distributions in the human proximal femur, Journal of Biomechanics 40 (11) (2007) 2573–2579. doi:10.1016/j.jbiomech.2006.11.022.

[48] B. E. C. Nordin, A. G. Need, B. E. Chatterton, M. Horowitz, H. A. Morris, The Relative Contributions of Age and Years since Menopause to Postmenopausal Bone Loss, J Clin Endocrinol Metab 70 (1) (1990) 83–88. doi:10.1210/jcem-70-1-83.

[49] L. F. Bonewald, Osteocytes as dynamic multifunctional cells, Annals of the New York Academy of Sciences 1116 (2007) 281–290. doi:10.1196/annals.1402.018.

[50] J. Klein-Nulend, A. D. Bakker, R. G. Bacabac, A. Vatsa, S. Weinbaum, Mechanosensation and transduction in osteocytes, Bone 54 (2) (2013) 182–190. doi:10.1016/j.bone.2012.10.013.

[51] T. Lemaire, J. Kaiser, S. Naili, V. Sansalone, Parametric study of interstitial fluid flow in the bone lacuno-canalicular network, Computer Methods in Biomechanics and Biomedical Engineering 15 (sup1) (2012) 331–332. doi:10.1080/10255842.2012.713683.

[52] S. Ramtani, Electro-mechanics of bone remodelling, International Journal of Engineering Science 46 (11) (2008) 1173–1182. doi:10.1016/j.ijengsci.2008.06.001.

[53] V. Sansalone, J. Kaiser, S. Naili, T. Lemaire, Interstitial fluid flow within bone canaliculi and electro-chemo-mechanical features of the canalicular milieu, Biomechanics and Modeling in Mechanobiology 12 (3) (2013) 533–553. doi:10.1007/s10237-012-0422-7.

[54] S. Scheiner, P. Pivonka, C. Hellmich, Poromicromechanics reveals that physiological bone strains induce osteocyte-stimulating lacunar pressure, Biomechanics and Modeling in Mechanobiology 15 (2016) 9–28. doi:10.1007/s10237-015-0704-y.

[55] J. S. Finkelstein, M.-L. T. Lee, M. Sowers, B. Ettinger, R. M. Neer, J. L. Kelsey, J. A. Cauley, M.-H. Huang, G. A. Greendale, Ethnic Variation in Bone Density in Premenopausal and Early Perimenopausal Women: Effects of Anthropometric and Lifestyle Factors, The Journal of Clinical Endocrinology & Metabolism 87 (7) (2002) 3057–3067. doi:10.1210/jcem.87.7.8654.

[56] M. Stolina, D. Dwyer, Q. T. Niu, K. S. Villasenor, P. Kurimoto, M. Grisanti, C. Y. Han, M. Liu, X. Li, M. S. Ominsky, H. Z. Ke, P. J. Kostenuik, Temporal changes in systemic and local expression of bone turnover markers during six months of sclerostin antibody administration to ovariectomized rats, Bone 67 (2014) 305–313. doi:10.1016/j.bone.2014.07.031.

[57] M. C. Peterson, M. M. Riggs, A physiologically based mathematical model of integrated calcium homeostasis and bone remodeling, Bone 46 (1) (2010) 49–63. doi:10.1016/j.bone.2009.08.053.

Table E.3: Nomenclature

Symbol	Description
	Cells
Ob_u, Ob_p, Ob_a	Osteoblast uncommited precursor cells, precursor cells, active osteoblasts
Oc_p, Oc_a	Osteoclast precursor cells, active osteoclasts
Ot	Osteocytes
η	Concentration of osteocytes in the bone matrix
	Ligands, hormones
LRP5/6	Lipoprotein receptor-related proteins 5/6
NO	Nitric oxide
OPG	Osteoprotegerin
PTH	Parathyroid hormone
RANK	Receptor activator of nuclear factor kappa-B
RANKL	Receptor activator of nuclear factor kappa-B ligand
Scl	Sclerostin
SclAb	Sclerostin monoclonal antibody
TGF-β	Transforming growth factor beta
	Mechanics
Ψ_{bm}	Strain energy density
f_{bm}	Volume fraction of bone matrix
BMD	Bone mineral density
	Pharmocokinetics
MM	Michaelis-Menten
PMO	Postmenopausal osteoporosis
PK	Pharmacokinetic
PD	Pharmacodynamic